Hindawi
International Journal of Photoenergy
Volume 2017, Article ID 4935265, 10 pages
https://doi.org/10.1155/2017/4935265

Research Article

Influence of the Porosity of the TiO_2 Film on the Performance of the Perovskite Solar Cell

Xiaodan Sun,[1] Jia Xu,[2] Li Xiao,[1] Jing Chen,[1,2] Bing Zhang,[1,3] Jianxi Yao,[1,2] and Songyuan Dai[1,3]

[1]*State Key Laboratory of Alternate Electrical Power System with Renewable Energy Sources, North China Electric Power University, Beijing 102206, China*
[2]*Beijing Key Laboratory of Energy Safety and Clean Utilization, North China Electric Power University, Beijing 102206, China*
[3]*Beijing Key Laboratory of Novel Film Solar Cell, North China Electric Power University, Beijing 102206, China*

Correspondence should be addressed to Jianxi Yao; jianxiyao@ncepu.edu.cn and Songyuan Dai; sydai@ipp.ac.cn

Received 8 October 2016; Accepted 19 December 2016; Published 1 February 2017

Academic Editor: Pushpa Pudasaini

The structure of mesoporous TiO_2 (mp-TiO_2) films is crucial to the performance of mesoporous perovskite solar cells (PSCs). In this study, we fabricated highly porous mp-TiO_2 films by doping polystyrene (PS) spheres in TiO_2 paste. The composition of the perovskite films was effectively improved by modifying the mass fraction of the PS spheres in the TiO_2 paste. Due to the high porosity of the mp-TiO_2 film, PbI_2 and CH_3NH_3I could sufficiently infiltrate into the network of the mp-TiO_2 film, which ensured a more complete transformation to $CH_3NH_3PbI_3$. The surface morphology of the mp-TiO_2 film and the photoelectric performance of the perovskite solar cells were investigated. The results showed that an increase in the porosity of the mp-TiO_2 film resulted in an improvement in the performance of the PSCs. The best device with the optimized mass fraction of 1.0 wt% PS in TiO_2 paste exhibited an efficiency of 12.69%, which is 25% higher than the efficiency of the PSCs without PS spheres.

1. Introduction

Perovskite solar cells based on $CH_3NH_3PbI_3$ have attracted much attention. Tremendous progress has been made since the seminal work of Kojima et al. in 2009 [1]. In just six years, power conversion efficiencies (PCEs) of PSCs have increased sharply from 3.8% [1] to 22.1% [2], which exceeds the PCEs of polycrystalline silicon solar cells [3–5]. Moreover, their solution processability and low cost endow them with high potential for next generation solar cells [4, 6].

Two typical PSC structures are widely used, including the planar heterojunction architectures [7] and the mesoporous structures [8–10]. Planar perovskite solar cells are advantageous because they have simple and scalable cell configurations [11]. In mesoporous structured PSCs, semiconductors, including TiO_2, ZnO, insulating Al_2O_3 and ZrO_2, are employed as the electron transporting layer (ETL) or the scaffold of the perovskite layer [12]. Due to its excellent physicochemical properties, such as large band gap, chemical stability, photostability, nontoxicity, and low cost [13], mesoporous TiO_2 is the most widely used electron transporting material in PSCs. The mp-TiO_2 film acts as not only the scaffold of the perovskite layer but also as the pathway for electron transport [14].

It has been reported that the structural properties of the mp-TiO_2 layer, such as particle size [15], thickness [16–18] and porosity, have a significant influence on the performance of PSCs [19]. Highly porous mp-TiO_2 films promote the easy infiltration of perovskite which subsequently fills the pores. A higher deposition of perovskites in mp-TiO_2 film results in increased light absorption and a higher current density [12, 14]. Moreover, the interface between the mp-TiO_2 film and perovskite film plays a key role in determining the overall conversion efficiency of PSCs [20]. Increasing the specific surface area and porosity of mp-TiO_2 film can promote a deeper infiltration of perovskites in TiO_2 films. This superior

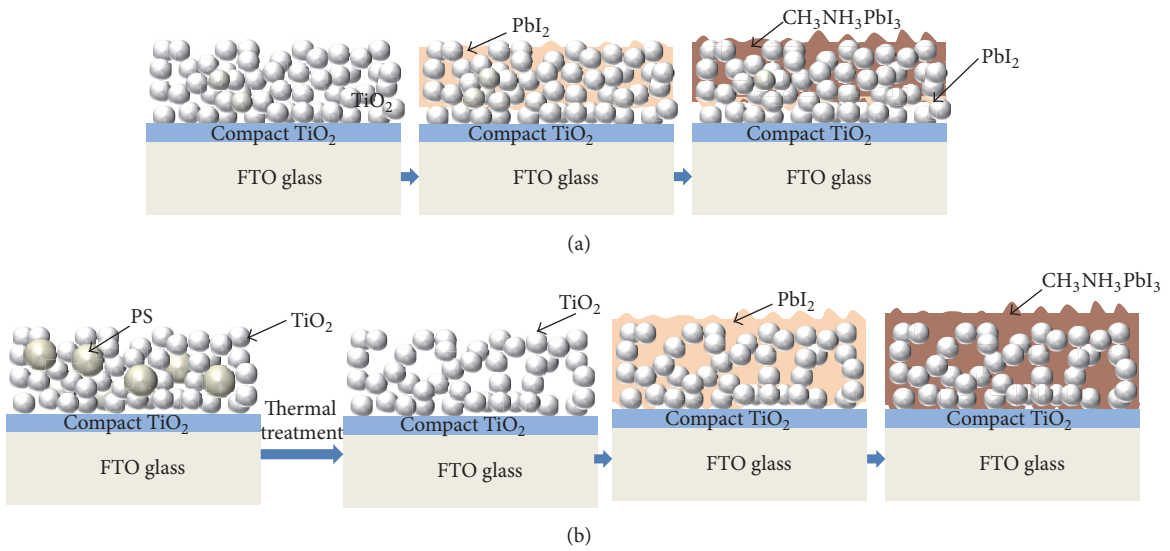

FIGURE 1: Schematic illustration of the distribution of PbI_2 and TiO_2 in mp-TiO_2 film (a) without and (b) with PS spheres.

infiltration is thought as an effective way to decrease the contact barrier between the $TiO_2/CH_3NH_3PbI_3$ interfaces, which could improve the transport of carriers in the PSCs. Dharani et al. [21] used electrospinning to prepare TiO_2 nanofibers as the ETL for PSCs. The TiO_2 nanofiber formed a highly porous structure. The excellent porous network resulted in improved loading of PbI_2. Therefore, the CH_3NH_3I can infiltrate through the pores to completely react with PbI_2. Sarkar et al. [22] prepared well-organized mesoporous TiO_2 photoelectrodes with enlarged pores by block copolymer-induced sol–gel assembly. TiO_2 photoelectrodes with larger pores are favorable for filling of perovskite in the mp-TiO_2 film. Within a certain range, devices based on larger pores showed a higher J_{sc} and superior performance. Rapsomanikis et al. [19] synthesized highly meso-macroporous TiO_2 thin films as ETLs of PSCs using a sol–gel process and Pluronic P-123 block copolymer as the organic template. Their results showed that the high porosity enabled the TiO_2 thin film to act as an ideal host for perovskite. The efficient contact between mp-TiO_2 and perovskite enhanced the electron transport.

Methods of controlling the mesoporous networks of mp-TiO_2 include changing the size of TiO_2 nanoparticles, using amphiphilic block copolymers [14, 22] and using templates. Many researchers reported that polystyrene (PS) spheres can be used as a mesostructured template to fabricate macro and mesoporous TiO_2 films in dye-sensitized solar cells (DSSC) because of its size tunability [23, 24]. By using various preparation method and PS spheres with different sizes, the morphology of the films can be easily controlled. Dionigi et al. [25] used PS spheres as structure-directing agents and coated the PS spheres with titanium dihydroxide to fabricate porous TiO_2 films with ordered pore architectures. Du et al. [24] fabricated hierarchically ordered macro-mesoporous TiO_2 films as the interfacial layer of DSSC using PS spheres as a template. Because of the periodically ordered structure and large specific surface of the macro-mesoporous TiO_2 films, a higher J_{sc} and a PCE enhanced by 83% were obtained.

However, to our knowledge, there have been no reports on the use of PS spheres to change the mesoporous networks of mp-TiO_2 film in PSCs. In this study, we present a facile method of controlling the porosity of mp-TiO_2 by introducing PS spheres into TiO_2 paste, which can be an effective strategy for the development of mesoporous PSCs. Figure 1 shows the schematic representation of the reaction process studied in this work. As shown in Figure 1(a), TiO_2 nanoparticles are close to each other. There are only few pores between the particles. PbI_2 cannot fully infiltrate into the narrow pores of mp-TiO_2 without the introduction of PS spheres during the preparation process; instead, CH_3NH_3I would react with the superficial PbI_2, which results in a large amount of residual PbI_2 in the TiO_2 film. In Figure 1(b), PS spheres can be observed in the TiO_2 film before heat treatment. Then PS spheres were removed by heat treatment and a large amount of pores were formed in mesoporous TiO_2 film. Therefore, more PbI_2 infiltrated into the film. The subsequently deposited CH_3NH_3I reacted more completely with PbI_2, which reduced the amount of the residual PbI_2. By adjusting the mass fraction of PS spheres in TiO_2 paste, a controllable porous mp-TiO_2 film was obtained. The incorporation of the macropores in mp-TiO_2 films increased the perovskite loading in the film and improved the contact between the TiO_2 and perovskite interface, which effectively suppressed charge recombination in the interface. X-ray diffraction and fluorescence lifetime measurements confirmed that the increased porosity ensured an adequate reaction between PbI_2 and CH_3NH_3I, thus decreasing the amount of residual PbI_2 and enhancing the electron injection from the perovskite to mp-TiO_2 film. The PSCs with the

porous TiO_2 films showed an enhanced short-circuit current density and higher efficiency.

2. Materials and Methods

2.1. Materials. Titanium dioxide paste (18-RT) was purchased from Yingkou OPV Tech New Energy Co., Ltd. Ethanol (99.8%) and hydrochloric acid (36%) were purchased from Beijing Chemical Plant (Beijing, China). The 100 nm PS spheres (Mw ~ 100000) were purchased from Janus New-Materials Co., Ltd. PbI_2 (99%) was purchased from Acros. CH_3NH_3I (99.5%) and 2,2′,7,7′-tetrakis-(N,N-dipmethoxyphenylamine)-9,9′-spirobifluorene (Spiro-OMeTAD) (99.7%) were purchased from Borun Chemicals (Ningbo, China). Tris(2-(1H-pyrazol-1-yl)-4-tert-butylpyridine)-cobalt(III)tris(bis(trifluoromethylsulfonyl)imide) (FK209-cobalt(III)-TFSI) was purchased from MaterWin Chemicals (Shanghai, China). N,N-dimethylformamide (DMF) was purchased from Alfa Aesar. Isopropanol was purchased from J&K Scientific Co., Ltd. All chemicals were used as received. Glass substrates with a transparent fluorine-doped tin oxide (FTO, sheet resistance 15 Ω/square) layer were used for the PSCs.

The solution of the compact TiO_2 is prepared by mixing titanium isopropoxide, HCl, and ethanol with a volume ratio of 7 : 22 : 100. In the solution of compact TiO_2, the concentrations of HCl and ethanol are 70.24% and 8.48%, respectively. For the preparation of the TiO_2 paste, we first diluted the TiO_2 paste in ethanol with a ratio of 1 : 3.5. Then, the mixture was added to 100 nm PS spheres with various wt% (0 wt%, 1.0 wt%, and 1.5 wt%) and stirred for 12 h. The spiro-MeOTAD solution was prepared by dissolving 72.3 mg spiro-MeOTAD in 1 mL chlorobenzene, and then 28.8 μL TBP and an 8 μL solution of LiTFSI (520 mg/mL LiTFSI in acetonitrile) were added.

2.2. Device Fabrication. Devices were fabricated on FTO glass substrates with a dimension of 1.5 cm × 1.3 cm. First, FTO was partially etched with Zn powder and HCl. Then, the etched FTO was cleaned using potassium sulfate solution, soap, deionized water, and ethanol, and, finally, it was sintered at 500°C for 30 minutes. A compact TiO_2 layer was prepared by spin coating compact TiO_2 solution, followed by annealing at 500°C for 30 min. The mesoporous TiO_2 film was prepared by spin coating 35 μL TiO_2 paste at 5000 r.p.m. for 30 s. Then, the films were heated to 450°C for 2 hours with a heating rate of 5°C/min. 462 mg of PbI_2 was dissolved in 1 mL DMF under stirring at 70°C for 12 hours. 40 μL PbI_2 solution was spin-coated on the mp-TiO_2 films at 3000 r.p.m. for 30 s. After loading was performed for 4 min, the substrates were dried at 70°C for 30 min. After the films were cooled to room temperature, 90 μL CH_3NH_3I solution in 2-propanol (8 mg/mL) was sprayed on the PbI_2 films, and the films were spun at 4000 r.p.m. for 30 s and then dried at 70°C for 30 min. The hole transporting layer (HTL) was prepared by spinning spiro-MeOTAD on the $TiO_2/CH_3NH_3PbI_3$ film at 3000 r.p.m. for 30 s. Finally, 70 nm gold electrodes were deposited on top of the device by thermally evaporation.

2.3. Characterization and Measurement. The surface morphology of the films was observed with a field emission scanning electron microscope (SEM, SU8010, Hitachi, 20.0 kV, 10.5 μA). The AFM images were obtained by An AC Mode III (Agilent 5500) atomic force microscope (AFM). X-ray diffraction (XRD) patterns were obtained by using a Bruker X-ray diffractometer with a Cu-Kα radiation source (40 kV, 400 mA). The 2θ diffraction angle was scanned from 10° to 80°, with a scanning speed of 1 second per step. The incident-photon-to-electron conversion efficiency (IPCE) curves were measured under ambient atmosphere using a QE-R measurement system (Enli Technology). The current-voltage characteristics (*J-V* curves) were obtained with a Keithley 2400 source meter and a sunlight simulator (XES-300T1, SAN-EI Electric, AM 1.5), which was calibrated using a standard silicon reference cell.

3. Results and Discussion

3.1. Morphology of the Porous TiO_2 Film. The size and mass fraction of PS spheres are crucial in determining the porosity and uniformity of the TiO_2 mesoporous layer. The surface morphology of the TiO_2 films was analyzed by scanning electron microscopy. The SEM images of sample PS-1.0 before and after heat treatment are shown in Figure S1 in Supplementary Material available online at https://doi.org/10.1155/2017/4935265. As observed in Figure 2, unlike the TiO_2 layer formed by spinning the paste without PS spheres (PS-0), pores can be observed in the mp-TiO_2 film prepared by TiO_2 paste with PS spheres. For a low mass fraction of 0.5 wt% PS spheres in the paste (PS-0.5), a few pores with an average size of 70 nm (the statistic numbers and histogram of pore size distribution are shown in Table S1 and Figure S2) are formed on the surface of the mp-TiO_2 layer. When the mass fraction of the PS spheres in TiO_2 paste increased to 1.0 wt%, (PS-1.0), lots of pores with an average size of 80 nm are formed. The average pore sizes for both PS-0.5 and PS-1.0 are almost the same, and the pore distribution is uniform. As the mass fraction of PS spheres increases to 1.5 wt% (PS-1.5), pores with relative larger pores (94 nm) were formed due to the high mass fraction of PS spheres and the agglomeration of PS spheres in the TiO_2 paste. The pore distribution is inhomogeneous compared to the PS-1.0 sample. The pore structure could be clearly observed in the cross-sectional SEM images of samples PS-0 and PS-1.0 (Figures 2(e) and 2(f)). As observed in Figures 2(e) and 2(f), the thickness of samples PS-0 and PS-1.0 is 260 nm and 360 nm, respectively. Moreover, the porous structure of sample PS-1.0 is looser than that of sample PS-0. The TiO_2 nanoparticles are densely packed and there are almost no pores among the nanoparticles in sample PS-0. However, pores can be observed from the cross-sectional SEM image in PS-1.0 (Figure 2(f)). The pores emerged not only on the surface of mp-TiO_2 film but also throughout the film. Sample

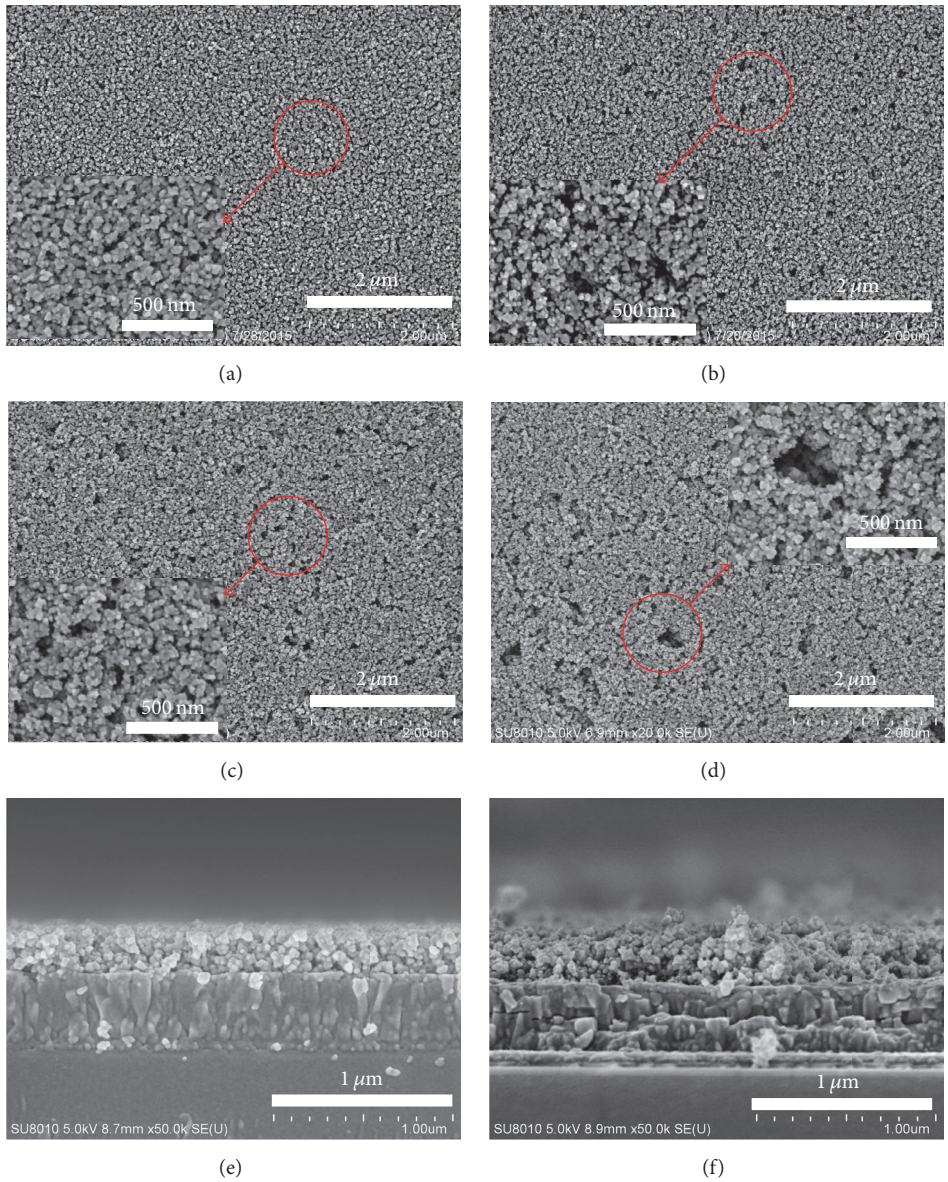

Figure 2: Plane-view SEM images of (a) PS-0, (b) PS-0.5, (c) PS-1.0, and (d) PS-1.5. Cross-sectional SEM images under high magnification of (e) PS-0 and (f) PS-1.0.

PS-1.0 is thicker than sample PS-0 due to the presence of more pores in the film.

3.2. Effect of TiO_2 Porosity on the Growth of Perovskite. The mp-TiO_2 film plays a key role in determining the structure of the perovskite layer. SEM and AFM images of the perovskite layer were obtained for mp-TiO_2 films prepared by TiO_2 paste with different mass fraction PS spheres. As shown in Figure 3, the average size of the perovskite is 300 nm regardless of if PS spheres were used in the mp-TiO_2 paste or not. The root-mean-square (RMS) roughness values of the $CH_3NH_3PbI_3$ films based on samples PS-0, PS-0.5, PS-1.0, and PS-1.5 obtained for a 5 μm × 5 μm area were evaluated as 53.3 nm, 55.6 nm, 53.2 nm, and 58.2 nm, respectively. This means that the amount of pores in the mp-TiO_2 films does not change the morphology and roughness of the perovskite film.

To better understand the distribution of perovskite in the mp-TiO_2 film, energy dispersive X-ray (EDX) mapping was performed. The EDX mapping of the cross-sectional area shows the distribution of two elements, Ti and Pb, along the mp-TiO_2 film thickness. As observed in Figure 4(a), a small amount of Pb is deposited in the sample PS-0. Figure 4(b) shows that more Pb is deposited at deeper levels in the sample PS-1.0 and the distribution of Pb is more uniform along the thickness of the TiO_2 film. In addition, $CH_3NH_3PbI_3$ was uniformly distributed in the mp-TiO_2 film owing to the presence of more pores.

Moreover, the perovskite crystallinity and the amount of residual PbI_2 are crucial to the performance of perovskite solar cells. It is well known that the residual PbI_2 layer exists

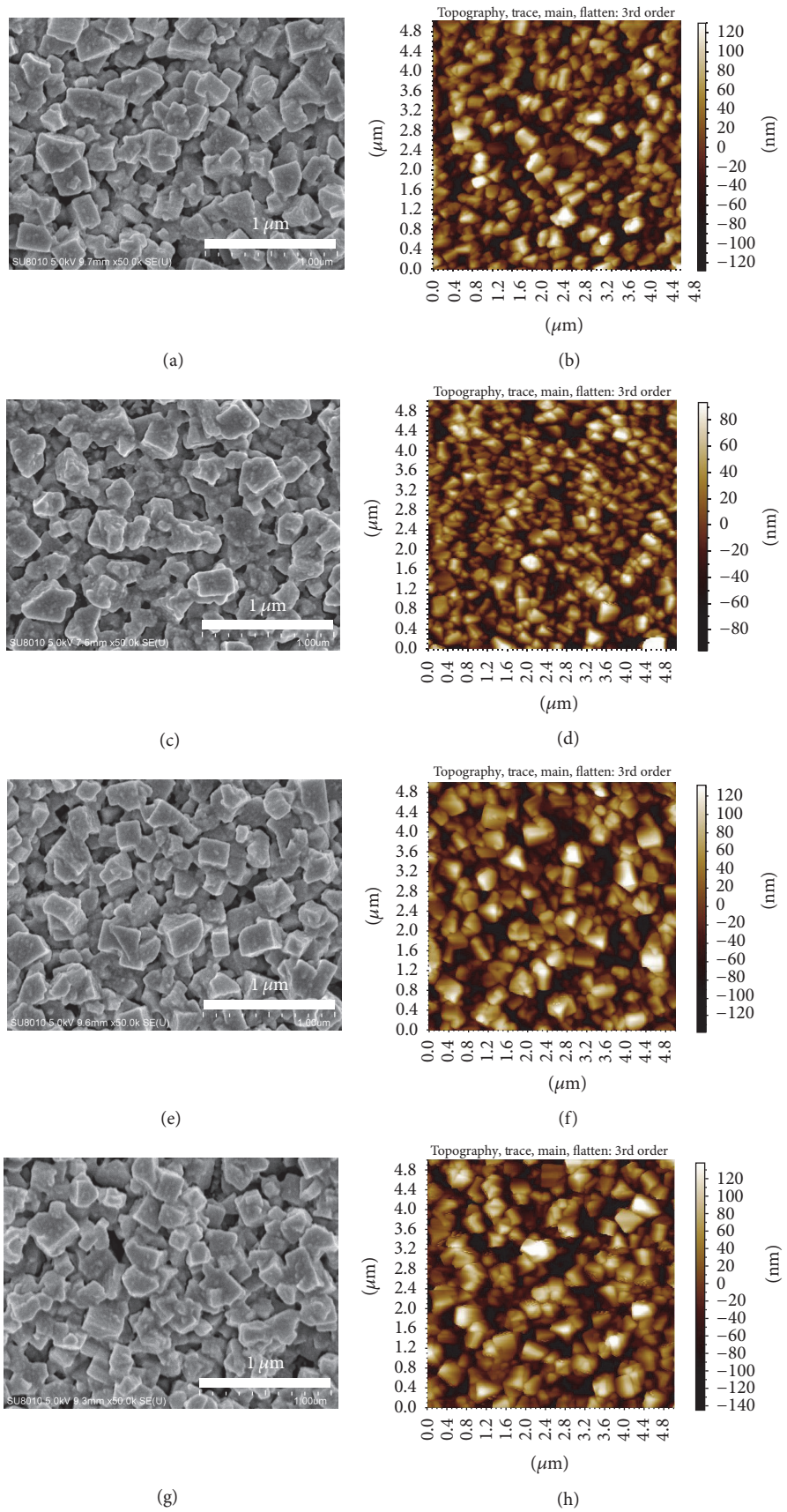

FIGURE 3: SEM and AFM images (5 μm × 5 μm) of the perovskite films based on the mesoporous TiO_2: (a), (b) PS-0; (c), (d) PS-0.5; (e), (f) PS-1.0; and (g), (h) PS-1.5.

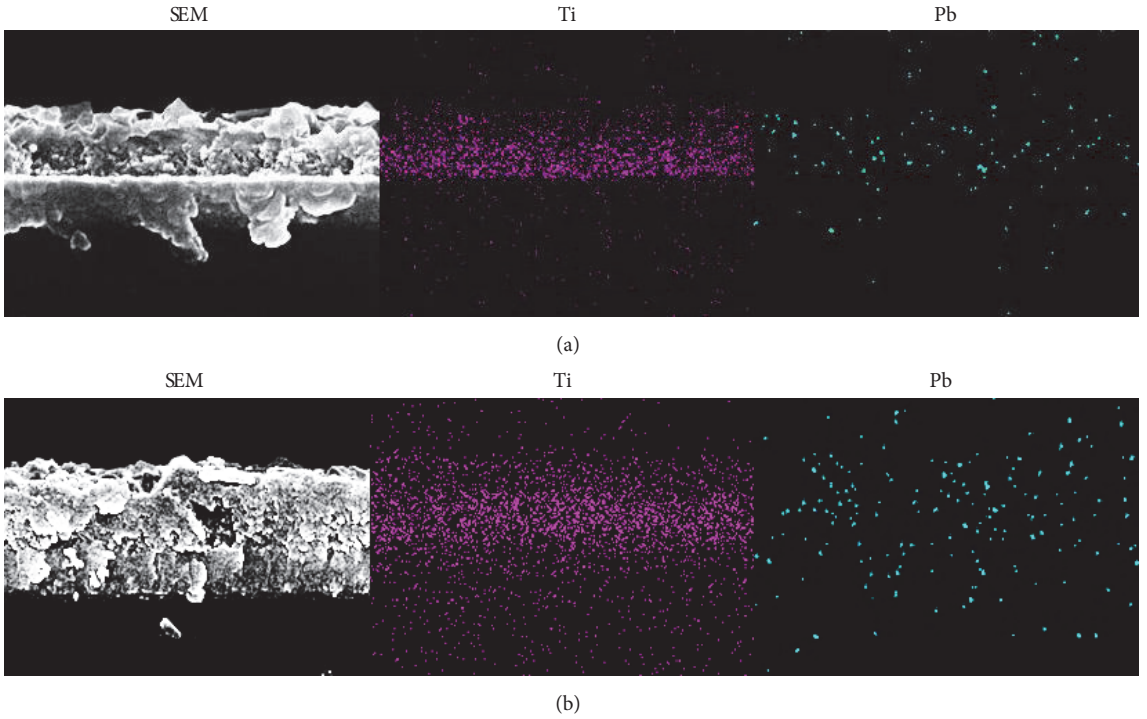

Figure 4: SEM-EDX mapping along the mp-TiO_2 film thickness to show the change in the distribution of Ti and Pb in $CH_3NH_3PbI_3$ loaded on (a) PS-0 and (b) PS-1.0.

between the interface of the mp-TiO_2 film and perovskite layer due to the incomplete reaction of PbI_2 and CH_3NH_3I [26]. Excessive amounts of residual PbI_2 will block the electron injected from the perovskite to mp-TiO_2 film, which deteriorates the cell performance of PSCs [27, 28]. However, a trace amount of residual PbI_2 acts as a passivation layer and reduces charge recombination at the interface between mp-TiO_2 film and the perovskite layer. To investigate the influence of the porosity of TiO_2 substrate on the growth of perovskite, X-ray diffraction was performed. In Figure 5, the peaks at 26.8°, 38.1°, and 51.8° correspond to the (110), (200), and (211) planes of FTO. The diffraction peaks marked by stars represent the PbI_2 (001) lattice plane, which conforms well with the literature data [29]. The Bragg peaks at 14.08°, 19.92°, 28.40°, 31.85°, 40.46°, and 43.02°, respectively, represent the reflections from the (110), (112), (220), (310), (224), and (314) crystal planes of the tetragonal perovskite structure [30, 31], which means that the change in porosity of the TiO_2 mesoporous layer has no influence on perovskite crystallinity. However, as the mass fraction of PS spheres in the TiO_2 paste increases, the intensity of the PbI_2 peaks reduces. There is only a little residual PbI_2 in the sample PS-1.0. By introducing PS spheres in TiO_2 paste, more pores were formed in the mp-TiO_2 film. The presence of more pores enables a deeper infiltration of PbI_2 and CH_3NH_3I solution, which endows complete reaction to $CH_3NH_3PbI_3$.

3.3. Photovoltaic Characterization of PSCs. The current density versus voltage (*J-V*) characteristics of PCSs based on the mp-TiO_2 layer prepared by TiO_2 paste with and without PS

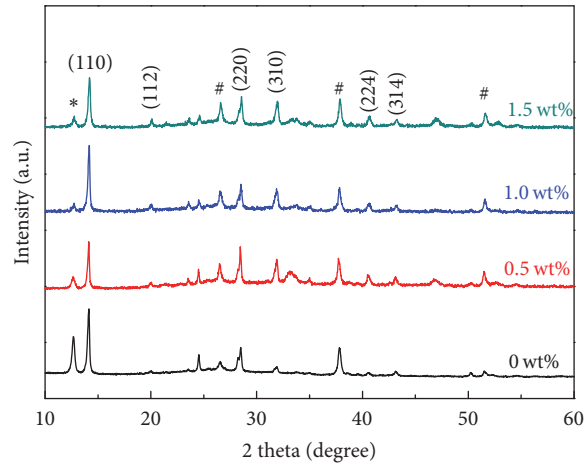

Figure 5: X-ray diffraction patterns of $CH_3NH_3PbI_3$ films based on TiO_2 mesoporous layers with different mass fractions of PS spheres.

spheres are shown in Figure 6. The photovoltaic parameters of the devices are summarized in Table 1. PSCs based on the mp-TiO_2 film PS-0 showed a reasonable PCE of 10.07% with an open-circuit voltage (V_{oc}) of 0.91 V, a short-circuit current (J_{sc}) of 19.07 mA/cm^2, and a fill factor (FF) of 57.99%. A relatively higher performance was exhibited by the device with PS spheres. After doping 0.5 wt% PS spheres, J_{sc}, V_{oc},

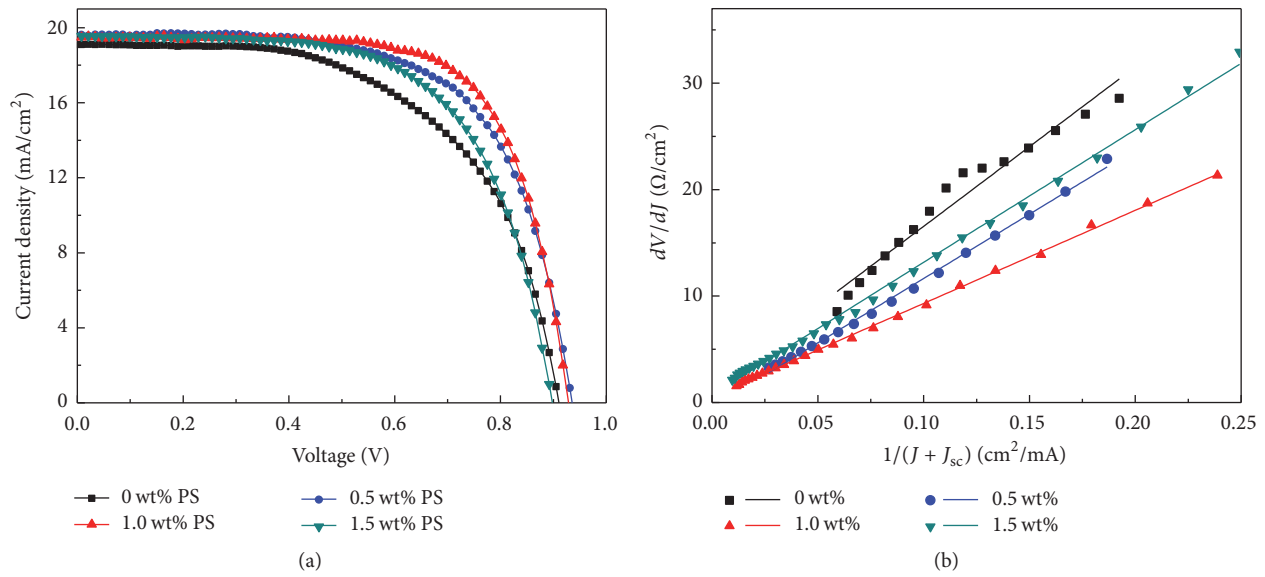

Figure 6: (a) Current density-voltage curves and the best-performing solar cells based on mp-TiO_2 film with different wt% of PS. (b) Plots of dV/dJ versus $1/(J + J_{sc})$ and the linear fitting curves.

Table 1: Photovoltaic performance of $CH_3NH_3PbI_3$ based devices as a function of different wt% of PS.

wt% of PS	R_{sh} (Ω)	R_s (Ω·cm^2)	J_{sc} (mA/cm^2)	V_{oc} (V)	Fill factor (%)	Efficiency (%)
0	1220	1.57	19.07	0.91	57.99	10.07
0.5	3860	0.43	19.64	0.94	64.91	11.92
1.0	5320	0.56	19.44	0.93	69.91	12.62
1.5	3700	0.71	19.54	0.90	63.47	11.14

FF, and PCE increased to 19.64 mA/cm^2, 0.94 V, 64.91% and 11.92%, respectively. For a 1.0% mass fraction of PS spheres, the best PCE (V_{oc} of 0.93, J_{sc} of 19.44 mA/cm^2, FF of 69.91%, and PCE of 12.62%) was achieved. When the mass fraction of PS spheres increased to 1.5 wt%, the PCS exhibits J_{sc} of 19.54 mA/cm^2, V_{oc} of 0.90 V, FF of 63.47%, and PCE of 11.14%. The decrease in the residual PbI_2 contributes to rapid electron injection from the perovskite to TiO_2 and higher J_{sc}. The improvements in the performance for the PSCs are mainly due to the increase of FF. Generally, FF depends largely on the series resistance (R_s) and shunt resistance (R_{sh}).

The equivalent circuit of the perovskite solar cell is shown in Figure 7. The output current density J can be expressed by the following equation:

$$J = J_0 \left(e^{q(V-JR_s)/AkT} - 1\right) + \frac{V - JR_s}{R_{sh}} - J_{sc}, \quad (1)$$

where J_0 represent the reverse saturation current density, A is ideality factor, k is Boltzmann's constant, T represent the temperature, and q represent electron charge. When $R_s \ll R_{sh}$, (1) can be expressed as

$$\frac{dV}{dJ} = R_s + \frac{AkT}{q}\frac{1}{J + J_{sc}}. \quad (2)$$

It is found that, from (2), dV/dJ has a linear relation with $(J_{sc} - J)^{-1}$. The intercept of the linear fitting curve gives the value of series resistance. Figure 6(b) shows the plot of dV/dJ versus $1/(J + J_{sc})$ and the linear fitting curve. As can be seen in Figure 6(b), the fitting curves are more linear by doping PS spheres in TiO_2 paste. Slightly decreased values of R_s from 1.57 Ω·cm^2 to 0.43 Ω·cm^2, 0.56 Ω·cm^2, and 0.71 Ω·cm^2 were evaluated after doping 0.5 wt%, 1.0 wt%, and 1.5 wt% PS spheres in the mp-TiO_2 paste. The smaller R_s values are due to the reduction in both the contact resistance and bulk resistance, which means a higher photocurrent will be generated [32]. However, when the mass fraction of PS spheres is 1.5 wt%, the increased R_s is attributed to the higher resistance caused by more pores and the negative contact with TiO_2 nanoparticles. The device based on TiO_2 mesoporous layer prepared by TiO_2 paste with PS spheres showed larger R_{sh} (R_{sh} values of the PSCs are 1220 Ω, 3860 Ω, 5320 Ω, and 3700 Ω for doping with 0 wt%, 0.5 wt%, 1.0 wt%, and 1.5 wt% PS spheres, resp.). A higher R_{sh} can improve FF and electron mobility [33], which is consistent with the results of the J-V test.

R_{sh} is closely related to the charge recombination at interfaces inside solar cells. A lower charge recombination contributes to a higher R_{sh} [34]. To better understand the separation of light-induced charge at the $TiO_2/CH_3NH_3PbI_3$ interface, we performed time-resolved photoluminescence (PL) decay measurements on the $CH_3NH_3PbI_3$ perovskite-filled mp-TiO_2 films prepared by TiO_2 paste with different

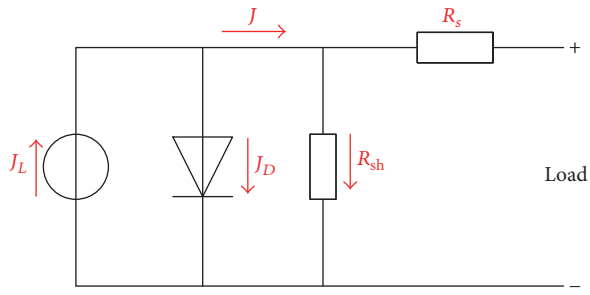

Figure 7: Equivalent circuit of the perovskite solar cell.

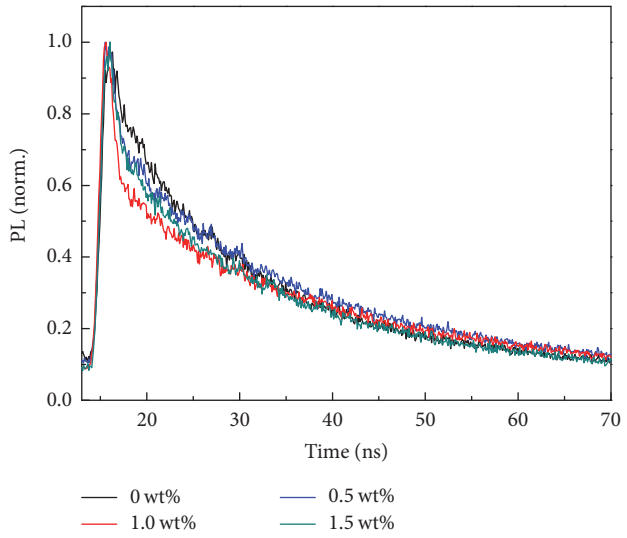

Figure 8: Normalized transient PL decay profiles of the perovskites based on TiO_2 with different wt% PS.

mass fractions of PS spheres, which are presented in Figure 8. Using global biexponential fits, the PL decay of the $CH_3NH_3PbI_3$ perovskite in the mp-TiO_2 films without PS spheres and with 0.5 wt%, 1.0 wt% and 1.5 wt% PS spheres exhibits τ_1 values of 22.53 ns, 17.57 ns, 17.71 ns, and 18.93 ns, respectively. By doping PS spheres into the TiO_2 paste, the rate of electron injection from the perovskite into TiO_2 film becomes faster, which results in lower charge recombination at the $TiO_2/CH_3NH_3PbI_3$ interfaces. This could be attributed to the better filling of the $CH_3NH_3PbI_3$ perovskite in the mp-TiO_2 film and the more complete contact between the TiO_2/perovskite as more pores emerge in the mp-TiO_2 film.

The photon-to-electron conversion efficiency (IPCE) spectra with mp-TiO_2 doping for different mass fractions of PS spheres are shown in Figure 9. The convolution of the spectral response with the photon flux of the AM 1.5G spectrum provided the estimated J_{sc} values of 15.537 mA/cm^2, 16.994 mA/cm^2, 16.825 mA/cm^2, and 16.397 mA/cm^2. The calculated J_{sc} values from the IPCE spectrum are well matched with the J_{sc} values obtained from the *J-V* curves. In addition, the PCSs from mp-TiO_2 films with PS spheres exhibited a higher and broader spectrum from 450 nm to 700 nm. Here, an IPCE of ~80% was obtained at the

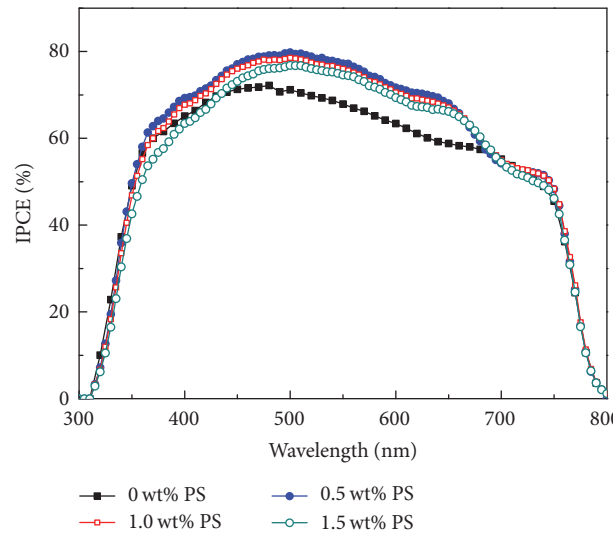

Figure 9: IPCE spectra of the best-performing solar cells based on different mass fractions of PS spheres.

maximum peak, while the device based on mp-TiO_2 films without PS spheres exhibited a lower IPCE of ~70%.

To further determine the influence of the porosity of mp-TiO_2 films on the fabricated solar cells, we showed the statistic results of the cells based on the mp-TiO_2 film prepared by TiO_2 paste with different mass fractions of PS spheres in Figure 10. The deviations of J_{sc}, V_{oc}, FF, and PCE have been shown in Table S2. As observed in Figure 10, J_{sc} and FF increase as the mass fraction of the PS spheres increases and they attain their highest values at the mass fraction of 1.0 wt%, which contributes to the increase in the PCE.

4. Conclusions

In conclusion, mp-TiO_2 films with tunable porosities were fabricated by doping PS spheres in TiO_2 paste and applied as the ETL of perovskite solar cells. The results indicate that the porosity of mp-TiO_2 films not only affects the infiltration and residual amounts of PbI_2 but also significantly influences the contact between the mp-TiO_2 film and perovskite layer. By adjusting the mass fraction of PS spheres, the perovskite solar cell based on mp-TiO_2 film prepared by TiO_2 paste with 1.0 wt% PS spheres exhibits the highest power conversion efficiency of 12.62% under a simulated standard AM 1.5 condition.

Competing Interests

The authors declare that they have no competing interests.

Acknowledgments

This work was supported by the National High Technology Research and Development Program of China (863 Program) (no. 2015AA050602), the National Natural Science Foundation of China (no. 51372083), Jiangsu Province Science and

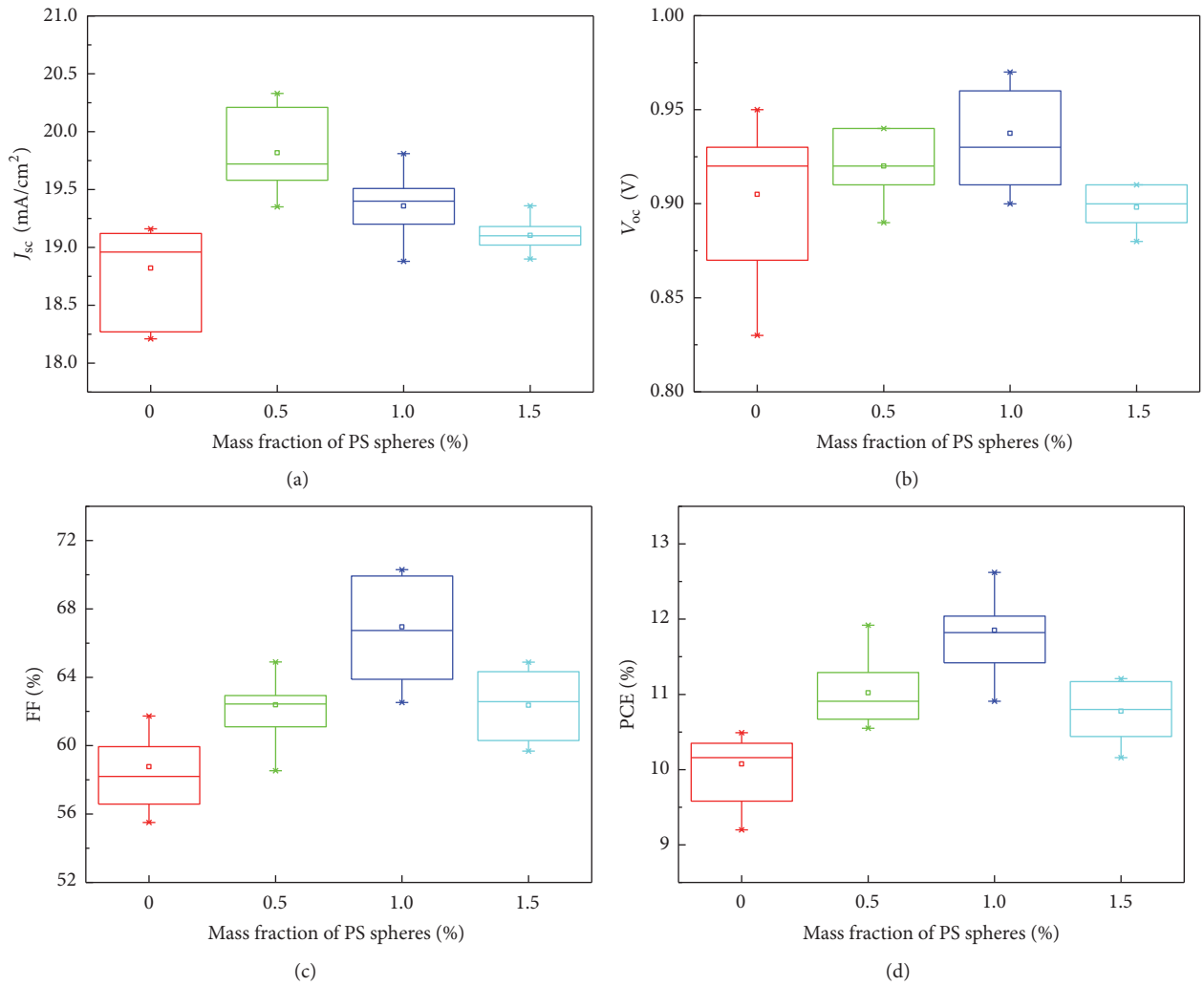

FIGURE 10: Statistic results of the cells based on the mp-TiO_2 film with different mass fractions of PS spheres.

Technology Support Program, China (BE2014147-4), and the Fundamental Research Funds for the Central Universities (nos. 2014ZZD07 and 2015ZD11).

References

[1] A. Kojima, K. Teshima, Y. Shirai, and T. Miyasaka, "Organometal halide perovskites as visible-light sensitizers for photovoltaic cells," *Journal of the American Chemical Society*, vol. 131, no. 17, pp. 6050–6051, 2009.

[2] "Best Research-Cell Efficiencie," national renewable energy laboratory, http://www.nrel.gov/pv/assets/images/efficiency_chart.jpg.

[3] W. S. Yang, J. H. Noh, N. J. Jeon et al., "High-performance photovoltaic perovskite layers fabricated through intramolecular exchange," *Science*, vol. 348, no. 6240, pp. 1234–1237, 2015.

[4] J. Qing, H.-T. Chandran, H.-T. Xue et al., "Simple fabrication of perovskite solar cells using lead acetate as lead source at low temperature," *Organic Electronics: physics, materials, applications*, vol. 27, article no. 3243, pp. 12–17, 2015.

[5] M. I. Ahmed, A. Habib, and S. S. Javaid, "Perovskite solar cells: potentials, challenges, and opportunities," *International Journal of Photoenergy*, vol. 2015, Article ID 592308, 13 pages, 2015.

[6] Q. Chen, H. Zhou, Z. Hong et al., "Planar heterojunction perovskite solar cells via vapor-assisted solution process," *Journal of the American Chemical Society*, vol. 136, no. 2, pp. 622–625, 2014.

[7] M. Liu, M. B. Johnston, and H. J. Snaith, "Efficient planar heterojunction perovskite solar cells by vapour deposition," *Nature*, vol. 501, no. 7467, pp. 395–398, 2013.

[8] L. Etgar, P. Gao, Z. Xue et al., "Mesoscopic $CH_3NH_3PbI_3/TiO_2$ heterojunction solar cells," *Journal of the American Chemical Society*, vol. 134, no. 42, pp. 17396–17399, 2012.

[9] H.-S. Kim, C.-R. Lee, J.-H. Im et al., "Lead iodide perovskite sensitized all-solid-state submicron thin film mesoscopic solar cell with efficiency exceeding 9%," *Scientific Reports*, vol. 2, article 591, 2012.

[10] M. M. Lee, J. Teuscher, T. Miyasaka, T. N. Murakami, and H. J. Snaith, "Efficient hybrid solar cells based on meso-superstructured organometal halide perovskites," *Science*, vol. 338, no. 6107, pp. 643–647, 2012.

[11] Y. Li, J. K. Cooper, R. Buonsanti et al., "Fabrication of planar heterojunction perovskite solar cells by controlled low-pressure vapor annealing," *Journal of Physical Chemistry Letters*, vol. 6, no. 3, pp. 493–499, 2015.

[12] H. Liu, Z. Huang, S. Wei, L. Zheng, L. Xiao, and Q. Gong, "Nano-structured electron transporting materials for perovskite solar cells," *Nanoscale*, vol. 8, no. 12, pp. 6209–6221, 2016.

[13] M. He, D. Zheng, M. Wang, C. Lin, and Z. Lin, "High efficiency perovskite solar cells: from complex nanostructure to planar heterojunction," *Journal of Materials Chemistry A*, vol. 2, no. 17, pp. 5994–6003, 2014.

[14] H. Lu, K. Deng, N. Yan et al., "Efficient perovskite solar cells based on novel three-dimensional TiO_2 network architectures," *Science Bulletin*, vol. 61, no. 10, pp. 778–786, 2016.

[15] Y. Yang, K. Ri, A. Mei et al., "The size effect of TiO_2 nanoparticles on a printable mesoscopic perovskite solar cell," *Journal of Materials Chemistry A*, vol. 3, no. 17, pp. 9103–9107, 2015.

[16] S. Aharon, S. Gamliel, B. E. Cohen, and L. Etgar, "Depletion region effect of highly efficient hole conductor free $CH_3NH_3PbI_3$ perovskite solar cells," *Physical Chemistry Chemical Physics*, vol. 16, no. 22, pp. 10512–10518, 2014.

[17] Y. Zhao, A. M. Nardes, and K. Zhu, "Solid-state mesostructured perovskite $CH_3NH_3PbI_3$ solar cells: charge transport, recombination, and diffusion lengt," *Journal of Physical Chemistry Letters*, vol. 5, no. 3, pp. 490–494, 2014.

[18] H.-S. Kim and N.-G. Park, "Parameters affecting I–V hysteresis of $CH_3NH_3PbI_3$ perovskite solar cells: effects of perovskite crystal size and mesoporous TiO2 layer," *Journal of Physical Chemistry Letters*, vol. 5, no. 17, pp. 2927–2934, 2014.

[19] A. Rapsomanikis, D. Karageorgopoulos, P. Lianos, and E. Stathatos, "High performance perovskite solar cells with functional highly porous TiO_2 thin films constructed in ambient air," *Solar Energy Materials and Solar Cells*, vol. 151, pp. 36–43, 2016.

[20] W. Wang, Z. Zhang, Y. Cai et al., "Enhanced performance of $CH_3NH_3PbI_{3-x}Cl_x$ perovskite solar cells by CH_3NH_3I modification of TiO_2-perovskite layer interface," *Nanoscale Research Letters*, vol. 11, no. 1, article 316, 2016.

[21] S. Dharani, H. K. Mulmudi, N. Yantara et al., "High efficiency electrospun TiO_2 nanofiber based hybrid organic–inorganic perovskite solar cell," *Nanoscale*, vol. 6, no. 3, pp. 1675–1679, 2014.

[22] A. Sarkar, N. J. Jeon, J. H. Noh, and S. I. Seok, "Well-organized mesoporous TiO_2 photoelectrodes by block copolymer-induced sol–Gel assembly for inorganic–organic hybrid perovskite solar cells," *Journal of Physical Chemistry C*, vol. 118, no. 30, pp. 16688–16693, 2014.

[23] Y. J. Kim, Y. H. Lee, M. H. Lee et al., "Formation of efficient dye-sensitized solar cells by introducing an interfacial layer of long-range ordered mesoporous TiO_2 thin film," *Langmuir*, vol. 24, no. 22, pp. 13225–13230, 2008.

[24] J. Du, X. Lai, N. Yang et al., "Hierarchically ordered macro–mesoporous TiO_2–graphene composite films: improved mass transfer, reduced charge recombination, and their enhanced photocatalytic activities," *ACS Nano*, vol. 5, no. 1, pp. 590–596, 2011.

[25] C. Dionigi, P. Greco, G. Ruani, M. Cavallini, F. Borgatti, and F. Biscarini, "3D hierarchical porous TiO_2 films from colloidal composite fluidic deposition," *Chemistry of Materials*, vol. 20, no. 22, pp. 7130–7135, 2008.

[26] S. Wang, W. Dong, X. Fang et al., "Credible evidence for the passivation effect of remnant PbI_2 in $CH_3NH_3PbI_3$ films in improving the performance of perovskite solar cells," *Nanoscale*, vol. 8, no. 12, pp. 6600–6608, 2016.

[27] Y. H. Lee, J. Luo, R. Humphry-Baker, P. Gao, M. Grätzel, and M. K. Nazeeruddin, "Unraveling the reasons for efficiency loss in perovskite solar cells," *Advanced Functional Materials*, vol. 25, no. 25, pp. 3925–3933, 2015.

[28] J. Jiang, H. J. Tao, S. Chen et al., "Efficiency enhancement of perovskite solar cells by fabricating as-prepared film before sequential spin-coating procedure," *Applied Surface Science*, vol. 371, pp. 289–295, 2016.

[29] D. H. Cao, C. C. Stoumpos, C. D. Malliakas et al., "Remnant Pbi2, an unforeseen necessity in high-efficiency hybrid perovskite-based solar cells? A)," *APL Materials*, vol. 2, no. 9, Article ID 091101, 2014.

[30] Y. Zhao and K. Zhu, "Charge transport and recombination in perovskite $(CH_3NH_3)PbI_3$ sensitized TiO_2 solar cells," *The Journal of Physical Chemistry Letters*, vol. 4, no. 17, pp. 2880–2884, 2013.

[31] T. Baikie, Y. Fang, J. M. Kadro et al., "Synthesis and crystal chemistry of the hybrid perovskite (CH3NH3)PbI3 for solid-state sensitised solar cell applications," *Journal of Materials Chemistry A*, vol. 1, no. 18, pp. 5628–5641, 2013.

[32] Y. Tu, J. Wu, M. Zheng et al., "TiO_2 quantum dots as superb compact block layers for high-performance $CH_3NH_3PbI_3$ perovskite solar cells with an efficiency of 16.97%," *Nanoscale*, vol. 7, no. 48, pp. 20539–20546, 2015.

[33] W. Ke, G. Fang, J. Wan et al., "Efficient hole-blocking layer-free planar halide perovskite thin-film solar cells," *Nature Communications*, vol. 6, article 6700, 2015.

[34] W. Ke, G. Fang, Q. Liu et al., "Low-temperature solution-processed tin oxide as an alternative electron transporting layer for efficient perovskite solar cells," *Journal of the American Chemical Society*, vol. 137, no. 21, pp. 6730–6733, 2015.